Results in Physics 2 (2012) 164–169

Contents lists available at SciVerse ScienceDirect

Results in Physics

journal homepage: www.journals.elsevier.com/results-in-physics

Quantum gravity on a laptop: 1 + 1 Dimensional Causal Dynamical Triangulation simulation

Norman S. Israel, John F. Lindner *

Physics Department, The College of Wooster, Wooster, Ohio, USA

ARTICLE INFO

Article history:
Received 9 August 2012
Accepted 5 October 2012
Available online 17 October 2012

Keywords:
Quantum gravity
Causal Dynamical Triangulation
Monte Carlo simulation

ABSTRACT

The quest for quantum gravity has been long and difficult. Causal Dynamical Triangulation is a new and straightforward approach to quantum gravity that recovers classical spacetime at large scales by enforcing causality at small scales. CDT combines quantum physics with general relativity in a Feynman sum-over-geometries and converts the sum into a discrete statistical physics problem. We solve this problem using a new Monte Carlo simulation to compute the spatial fluctuations of an empty universe with one space and one time dimensions. Our results compare favorably with theory and provide an accessible but detailed introduction to quantum gravity via a simulation that runs on a laptop computer.

1. Introduction

The long search for a satisfactory theory of quantum gravity has been beset by conceptual and technical problems, and the subject is complicated enough to discourage physicists from other fields from following its development, except superficially. However, in recent popular expositions [1,2], Jan Ambjørn, Jerzy Jurkiewicz, and Renate Loll (AJL) claim that one promising approach to quantum gravity, called Causal Dynamical Triangulation (CDT), is straightforward enough to simulate on a laptop computer. In this paper, we provide the background and technical details to do precisely that. In the simplest case of an empty universe of one spatial and one temporal dimension, we simulate a quantum universe on a laptop. While independently verifying theoretical predictions, we introduce and motivate key ideas and tools common to many approaches to quantum gravity and provide an accessible entry into the subject.

This paper is structured as follows. Section 2 places CDT in the context of other approaches to quantum gravity. Section 3 reviews classical gravity and quantum mechanics via principles of stationary action and combine them to form a propagator for quantum gravity. It motivates the Gauss–Bonnet theorem, Wick rotations, and Regge calculus to simplify the propagator by converting it to a partition function. Section 4 studies the corresponding statistical physics problem using Monte Carlo methods and highlights a phase transition at a critical cosmological constant. It reports the results of numerical simulations of the phase transition and of the quantum fluctuations of the universe's spatial size and compares them with theoretical predictions. Section 5 suggests possible improvements and future challenges.

Unless otherwise noted, we work in 1 + 1 spacetime dimensions and use natural Planck units where $G = c = \hbar = 1$. We place function arguments inside square brackets [...] and group terms for multiplication with round parentheses (...).

2. Quantum gravity

Theories of quantum gravity [3] attempt to unify quantum theory with general relativity, the theory of classical gravity as spacetime curvature. Superstring theory ambitiously tries to unify gravity with the electromagnetic and weak and strong nuclear interactions, but it requires supersymmetry and higher dimensions, which are as yet unobserved. It proposes that elementary particles are vibrational modes of "strings" of the Planck length ($\sim 10^{-33}$ cm), and classical spacetime is a coherent oscillation of "graviton" modes. Loop quantum gravity does not attempt to unify gravity with the other forces, but it directly merges quantum theory and general relativity to conclude that space is granular at the Planck scale. It proposes that space is a superposition of networks of quantised "loops", and spacetime is a discrete history of such networks.

Causal Dynamical Triangulation [4] is a conservative approach to quantum gravity that constructs spacetime from triangular-like building blocks by gluing their time-like edges in the same direction. The microscopic causality inherent in the resulting spacetime foliation ensures macroscopic space and time as we know it. Despite the discrete foundation, CDT does not necessarily imply that spacetime itself is discrete. It merely grows a combinatorial spacetime from the building blocks according to a propagator fashioned

* Corresponding author. Tel.: +1 330 263 2120; fax: +1 330 263 2516.
E-mail address: jlindner@wooster.edu (J.F. Lindner).

2211-3797
http://dx.doi.org/10.1016/j.rinp.2012.10.001

from a sum-over-histories superposition. Dynamically generating a classical universe from quantum fluctuations is an outstanding accomplishment of this approach.

CDT recovers classical gravity at large scales [5,6], but predicts that the number of dimensions drops continuously from 4 to 2 at small scales. To its credit, CDT's prediction of a nonclassical dimension of 2 near the Planck scale is potentially falsifiable. In fact, an earlier version of the theory, called Euclidean Dynamical Triangulation (EDT), has been falsified because it does not recover classical gravity at large scales. Furthermore, other approaches to quantum gravity [7,8] have subsequently predicted similar dimensional reductions from 4 to 2 near the Planck scale, which if confirmed would be a profound insight into the nature of space and time.

Previously published CDT work by AJL includes analytical results in 1 + 1 dimensions [9] and numerical results in 3 + 1 dimensions [5]. Additional work by Benedetti and Henson includes numerical results in 2 + 1 dimensions [10], but using the AJL Monte Carlo code. Here, after motivating the background theory, we provide detailed numerical methods and results from a new and independent Monte Carlo simulation in 1 + 1 dimensions to compare with the analytical results and provide a foundation for future work.

3. Background theory

3.1. Classical gravity

In the theory of relativity, space x and time t are on equal footing and mix when boosting between reference frames in relative motion. In the flat Minkowski spacetime of special relativity, the invariant proper space $d\sigma$ and time $d\tau$ between two nearby events follow from the generalised pythagorean theorem

$$+d\sigma^2 = dx^2 - dt^2 = -d\tau^2, \tag{1}$$

which involves the difference in the squares of the relative space dx and time dt between the events in some reference frame. This difference prevents causality violation, like walking back to yesterday, because light cones defined by $d\sigma = 0$ or $dt = \pm dx$ partition spacetime into invariant sets of past and future at each event. Free particles follow straight trajectories or world-lines $x[t]$ of stationary proper time.

In the curved spacetime of general relativity, the separation between two events follows from

$$d\sigma^2 = g_{xx}dx^2 + g_{xt}dx\ dt + g_{tx}dt\ dx + g_{tt}dt^2, \tag{2}$$

where the metric $g_{\mu\nu}$ encodes the spacetime geometry. Free particles follow curved world-lines of stationary proper time.

The vacuum gravitational field equations can be derived from the Einstein-Hilbert scalar action

$$S[g_{\mu\nu}] = \frac{1}{8\pi}\int da(K[g_{\mu\nu}] - \Lambda), \tag{3}$$

where the Gaussian curvature (described below) is half the Ricci scalar curvature, $K = R/2$, and Λ is the cosmological constant. By diagonalising the metric, the invariant area element

$$da = \sqrt{-g_{tt}}\ dt\ \sqrt{g_{xx}}\ dx = \sqrt{-g}\ dx\ dt, \tag{4}$$

where $g = \det g_{\mu\nu}$. Demanding that the action be stationary with respect to the metric, $\delta S/\delta g^{\mu\nu} = 0$, implies the gravitational field equations [11]

$$G_{\mu\nu} = R_{\mu\nu} - \frac{1}{2}g_{\mu\nu}R = -\Lambda g_{\mu\nu}, \tag{5}$$

where the Ricci tensor curvature is the variation of the Ricci scalar with the metric, $R_{\mu\nu} = \delta R/\delta g^{\mu\nu}$. The Einstein curvature $G_{\mu\nu}$ is proportional to the cosmological constant Λ, which can be interpreted as the vacuum energy density.

3.2. Quantum mechanics

In classical mechanics, the action

$$S_c[x] = \int dt\ (T - V[x]) \tag{6}$$

is the cumulative difference between a particle's kinetic energy T and potential energy $V[x]$. A particle of mass m follows a worldline $x[t]$ of stationary action. Demanding that the action be stationary with respect to the worldline, $\delta S_c/\delta x = 0$, implies Newton's equation

$$m\frac{d^2x}{dt^2} = F_x = -\frac{dV}{dx}. \tag{7}$$

In quantum mechanics, a particle follows all worldlines. Along each worldline, it accumulates a complex amplitude whose modulus is unity and whose phase is the classical action $S[x]$ in units of the quantum of action $\hbar$. The Feynman propagator, or amplitude to transition from place a to place b, is the sum-over-histories [12,13] superposition

$$A[a \to b] = \int \mathcal{D}x[t]\ e^{iS_c[x[t]]/\hbar} = \int \mathcal{D}x\ e^{iS_c[x]}, \tag{8}$$

where $\mathcal{D}x$ denotes the integration measure. The corresponding probability:

$$\mathcal{P} = |A|^2 \tag{9}$$

is the absolute square of the amplitude. If the wave function $\Psi[b] = A[a \to b]$ is the amplitude to be at a place b, and the kinetic energy $T = (1/2)m(dx/dt)^2$, then the path integral between infinitesimally separated places implies the nonrelativistic Schrödinger wave equation

$$H\Psi = -\frac{1}{2m}\frac{\partial^2\Psi}{\partial x^2} + V\Psi = i\frac{\partial\Psi}{\partial t}. \tag{10}$$

In quantum gravity, the corresponding sum is over all spacetime geometries $g_{\mu\nu}$, as suggested by Fig. 1, and the quantum phase of each geometry is the Eq. (3) Einstein-Hilbert action. The probability amplitude to transition from one spatial geometry to another is

$$A\left[g^a_{xx} \to g^b_{xx}\right] = \int \mathcal{D}g\ e^{iS[g_{\mu\nu}]}. \tag{11}$$

If $\Psi[g_{\mu\nu}]$ is the probability amplitude of a particular spatial geometry, then this path integral implies the timeless Wheeler-DeWitt equation [14]

$$\widetilde{H}\Psi = 0. \tag{12}$$

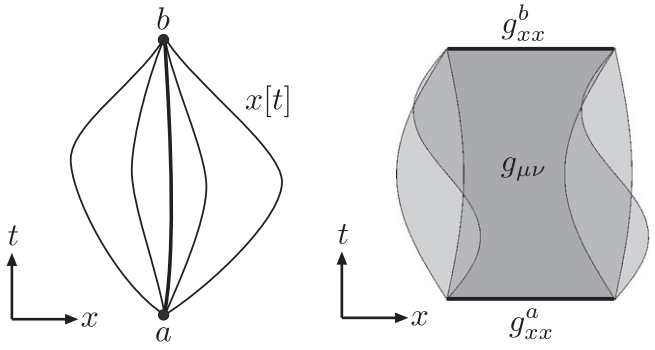

Fig. 1. Sum over histories in quantum mechanics (left) and quantum gravity (right). Virtual paths interpolate between places, and virtual spacetime geometries interpolate between spaces.

3.3. Gauss–Bonnet theorem

In 1 + 1 = 2 dimensions, the beautiful Gauss–Bonnet theorem [15] dramatically simplifies the Einstein-Hilbert action by relating the total curvature of an orientable closed surface to a topological invariant. The curvature of a hexahedron or cube is concentrated at its corners, as in Fig. 2, where the deficit angle

$$\epsilon = 2\pi - \sum_{n=1}^{3} \frac{\pi}{2} = \frac{\pi}{2}, \tag{13}$$

and the total curvature

$$K_T = \sum_{v=1}^{8} a_v K_v = \sum_{v=1}^{8} a_v \frac{\epsilon_v}{a_v} = \sum_{v=1}^{8} \epsilon_v = 8\left(\frac{\pi}{2}\right) = 4\pi, \tag{14}$$

where $K_v = \epsilon_v / a_v$ is the discrete Gaussian curvature at vertex v, and a_v is the area closer to that vertex than any other.

The Gaussian curvature of a circle of radius r is the reciprocal of its radius $1/r$. The Gaussian curvature at a point on a surface is the product of the corresponding minimum and maximum sectional curvatures. Hence, the total curvature of a sphere

$$K_T = \int da\, K = 4\pi r^2 \left(\frac{1}{r} \times \frac{1}{r}\right) = 4\pi, \tag{15}$$

just like the topologically equivalent cube. More generally,

$$K_T = \int da\, K = 2\pi\chi = 4\pi(1 - \mathcal{G}), \tag{16}$$

where χ is the surface's Euler characteristic and the genus $\mathcal{G}$ is its number of holes. For a sphere $\mathcal{G} = 0$, and for a torus $\mathcal{G} = 1$. Total curvature can only change discretely and only by changing the number of holes.

3.4. Wick rotation

The Eq. (11) sum over histories path integral is difficult to evaluate because of the oscillatory nature of its integrand. A Wick rotation [16] converts this difficult problem in Minkowski spacetime to a simpler one in Euclidean space by introducing an imaginary time coordinate. For example,

$$t \to -it_E. \tag{17}$$

One motivation for the Wick rotation comes from complex analysis, where the integral of an analytic function $f[z]$ around a closed curve in the complex plane always vanishes [17]. If the function also decreases sufficiently rapidly at infinity, then around the Fig. 3 contour C,

$$0 = \oint_C dz\, f[z] = \int_{-\infty}^{\infty} dz\, f[z] + 0 + \int_{i\infty}^{-i\infty} dz\, f[z] + 0, \tag{18}$$

and so

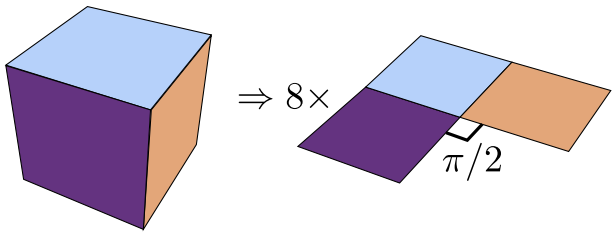

Fig. 2. Curvature of a polyhedron like a cube (left) is concentrated at its vertices and quantified by the degree to which the angles at a vertex fail to add up to a full circle (right).

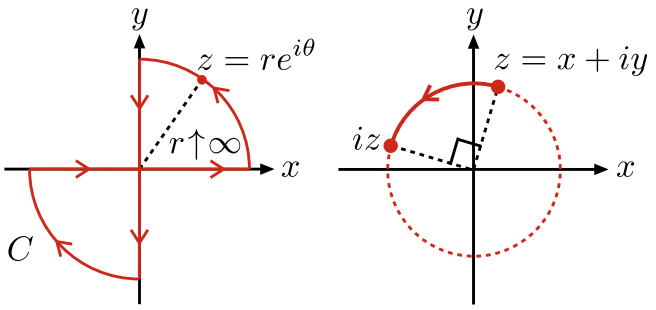

Fig. 3. Integration contour (left) and multiplication by i (right) in the complex plane motivate the Wick rotation.

$$\int_{-\infty}^{\infty} dx\, f[x] = i \int_{-\infty}^{\infty} dy\, f[iy], \tag{19}$$

which effectively rotates the integration 90° in the complex plane. Multiplying a complex number by $i = e^{i\pi/2}$ similarly rotates the number 90° in the complex plane.

The Eq. (17) Wick rotation maps the Eq. (1) line element by

$$d\sigma^2 = dx^2 - dt^2 \to dx^2 + dt_E^2 = d\sigma_E^2, \tag{20}$$

and hence the metric determinant by $-g \to g_E$ and the Eq. (4) area element by

$$da = \sqrt{-g}\, dx\, dt \to -i\sqrt{g_E}\, dx\, dt_E = -i\, da_E. \tag{21}$$

This maps the Eq. (3) Einstein-Hilbert action by

$$S = \frac{1}{8\pi} \int da(K - \Lambda) \to -i \frac{1}{8\pi} \int da_E (K - \Lambda) = -iS_E, \tag{22}$$

which maps the Eq. (11) probability amplitude by

$$A = \int \mathcal{D}g\, e^{iS} \to \int \mathcal{D}g\, e^{S_E} = Z. \tag{23}$$

This Wick rotation converts the Feynman phase factor e^{iS} to the Boltzmann weight $e^{S_E} = e^{-|S_E|}$, thereby connecting quantum and statistical mechanics, where toroidal boundary conditions and a positive cosmological constant $\Lambda > 0$ ensure (in Eq. (30) below) the negativity of the Euclidean action $S_E < 0$. The Eq. (23) notation Z for Zustandssumme (state sum) traditionally denotes the partition function, but the exponent is proportional to the action $S_E/\hbar$ rather than the energy per temperature E/k_BT.

3.5. Regge calculus

Triangulation can simplify the continuum to the discrete. The Fig. 4 equilateral Euclidean triangle of side $d\sigma = \ell$ and half-base $dx = \ell/2$ has height

$$dy = \sqrt{d\sigma^2 - dx^2} = \ell \frac{\sqrt{3}}{2} \tag{24}$$

and area

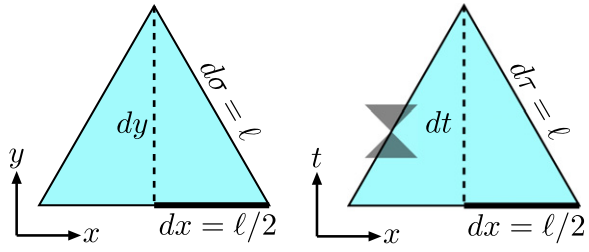

Fig. 4. Euclidean (left) and Minkowski (right) equilateral triangles. The time-like edges of the latter pass through past and future light cones.

$$a_E = \frac{1}{2} dx\ dy = \ell^2 \frac{\sqrt{3}}{4}. \tag{25}$$

In contrast, the Fig. 4 equilateral Minkowski triangle of time-like sides $d\tau = \ell$ and space-like half-base $dx = \ell/2$ has height

$$dt = \sqrt{d\sigma^2 + dx^2} = \ell \frac{\sqrt{5}}{2} \tag{26}$$

and area

$$a_M = \frac{1}{2} dx\ dt = \ell^2 \frac{\sqrt{5}}{4}. \tag{27}$$

Regge calculus [18] approximates curved spacetime by flat Minkowski triangles (or simplexes in higher dimensions) whose edge lengths ℓ may ultimately be shrunk to zero to recover a continuum theory. Curvature is concentrated in the deficit angles at the vertices. Dynamical Triangulation uses only equilateral triangles, but incorporates both positive and negative curvature by suitably gluing the triangles together. Causal Dynamical Triangulations uses only dynamical triangulations with a sliced or foliated structure with the time-like edges glued in the same direction, as in Fig. 5. Local light cones match to enforce global causality and preclude closed time-like curves (and hence backward-in-time travel).

Regge calculus and the Gauss–Bonnet theorem dramatically simplifies the Eq. (22) Wick-rotated Euclidean action from

$$S_E = \frac{1}{8\pi} \int da_E (K - \Lambda) \tag{28}$$

to

$$S_{E,R} = \frac{1}{8\pi} (2\pi\chi - N_\Delta a_E \Lambda), \tag{29}$$

where N_Δ is the number of triangles. Assuming periodic boundary conditions in space and time, so the model universe is toroidal with genus $\mathcal{G} = 1$, the Eq. (16) Euler characteristic $\chi = 2(1 - \mathcal{G}) = 0$, and the action

$$S_{E,R} = -\Lambda' N_\Delta < 0, \tag{30}$$

where the rescaled cosmological constant

$$\Lambda' = \Lambda \frac{a_E}{8\pi} = \Lambda \frac{a_M}{8\pi} \sqrt{\frac{3}{5}} > 0. \tag{31}$$

The integral in the Eq. (23) amplitude becomes the sums

$$Z_R = \sum e^{S_{E,R}} = \sum_{\text{CDT}} e^{-\Lambda' N_\Delta} = \sum_{\mathcal{T} \in \mathcal{T}_N} \frac{1}{C_\mathcal{T}} e^{-\Lambda' N_\Delta} = \sum_v \frac{1}{N_v!} e^{-2\Lambda' N_v}. \tag{32}$$

The second sum is over inequivalent causal dynamical triangulations. The third sum is over unlabeled triangulations, and the symmetry factor in the denominator corrects for over counting the $C_\mathcal{T}$ permutations of labelled vertices that preserve neighbor assignments. (For example, if 2 triangles are glued along their edges back-to-back, 1 set of $C_\mathcal{T} = 3! = 6$ permutations preserve the neighbor assignments; if 3 triangles are glued along their edges in a tetrahedron, 2 mirror-reversed sets of $C_\mathcal{T} = 4!/2 = 12$ permutations preserve the neighbor assignments.) The fourth sum is over labelled triangulations, where the factorial in the denominator corrects for over counting the $N_v!$ permutations of each triangulation's vertex labels. The number of triangles is twice the number of vertices, $N_\Delta = 2N_v$, because the Fig. 5 initial unit cell consists of two triangles and one vertex and all other triangulations are reached by rearrangements (described below) that add or subtract two triangles for each vertex.

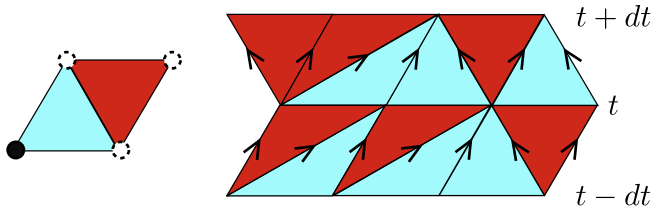

Fig. 5. Initial unit cell (left) and a partial triangulation (right). Arrows point toward the future of time-like edges. The equilateral Minkowski triangles are distorted because the triangulation is flattened into a Euclidean plane.

4. Simulation

4.1. Monte Carlo analysis

To analyse the statistical physics system defined by the Eq. (32) effective partition function, take a random walk through triangulation space sampling different geometries. The Fig. 6 move and its inverse are thought to be ergodic triangulation rearrangements. They are special cases of the Alexander moves of combinatorial topology [19]. The move $\mathcal{M}$ splits a vertex into two at the same time slice and adds two triangles, while its inverse $\mathcal{M}^{-1}$ fuses two vertices at the same time slice and deletes two triangles. Both preserve the foliation of the spacetime.

Monte Carlo sampling of the triangulations leads to a detailed balance in which moves equilibrate inverse moves. At equilibrium, the probability to be in a specific labelled triangulation of N_v vertices times probability to transition to a triangulation of $N_v + 1$ vertices satisfies

$$\mathcal{P}[N_v]\mathcal{P}[N_v \to N_v + 1] = \mathcal{P}[N_v + 1]\mathcal{P}[N_v + 1 \to N_v]. \tag{33}$$

After choosing to make a move, randomly select a vertex from N_v vertices, and then randomly split one of n_p past time-like edges and one of n_f future time-like edges, as in Fig. 6. Hence the move transition probability

$$\mathcal{P}[N_v \to N_v + 1] = \mathcal{P}[\mathcal{M}] \times \frac{1}{N_v} \times \frac{1}{n_p} \times \frac{1}{n_f}. \tag{34}$$

After choosing to make an inverse move, fusing the split vertices is the only way to return to the original triangulation. Hence the inverse move transition probability

$$\mathcal{P}[N_v + 1 \to N_v] = \mathcal{P}[\mathcal{M}^{-1}] \times 1, \tag{35}$$

By the Eq. (32) effective partition function, the probability of a labelled triangulation with N_v vertices is the weighted Boltzmann factor

$$\mathcal{P}[N_v] = \frac{1}{N_v!} \frac{e^{-2\Lambda' N_v}}{Z_R}. \tag{36}$$

The probability of a move is a non-unique choice. In our simulations, we choose

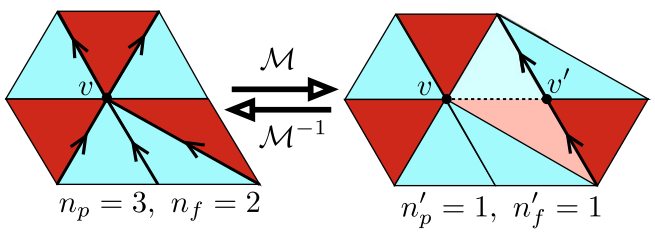

Fig. 6. Monte Carlo sequence of rearrangements ergodically samples different triangulations and hence different geometries.

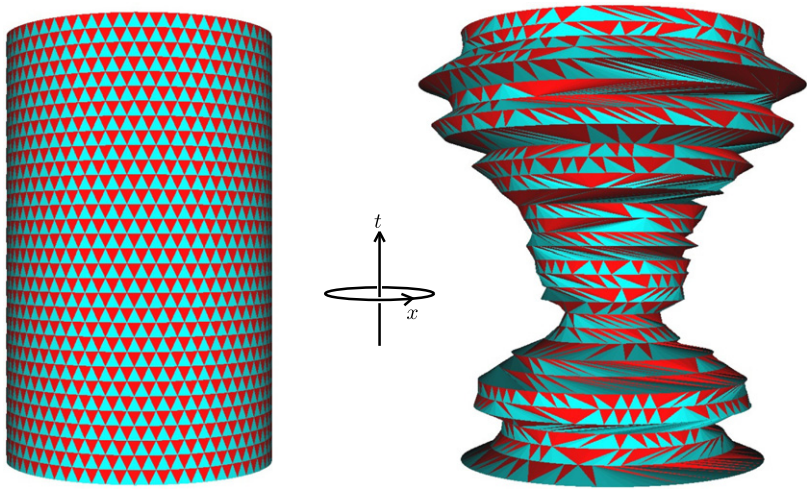

Fig. 7. Beginning with a homogeneous 1 + 1 dimensional universe (left), large vacuum fluctuations in circumference arise (right).

$$\mathcal{P}[\mathcal{M}] = \frac{N_v}{N_v + 1} \frac{n_p n_f}{n'_p + n'_f} e^{-\Lambda'}. \tag{37}$$

To satisfy the Eq. (33) detailed balance, the probability of an inverse move is therefore

$$\mathcal{P}[\mathcal{M}^{-1}] = \frac{1}{n'_p + n'_f} e^{+\Lambda'}. \tag{38}$$

Other choices may improve or worsen computational efficiency [20]. In practice, a Metropolis algorithm [21] accepts the rearrangements if these probabilities are greater than a uniformly distributed pseudo-random number between 0 and 1. For example, if $\mathcal{P}[\mathcal{M}] = 0.01$, then the move is unlikely to be accepted.

During the random walk through geometries, compute the averages of observables $\mathcal{O}$ using

$$\langle \mathcal{O} \rangle = \frac{1}{Z_R} \sum\nolimits_{\text{CDT}} \mathcal{O}_\Delta e^{-\Lambda' N_\Delta} = \frac{\sum \mathcal{O}_\Delta e^{-\Lambda' N_\Delta}}{\sum e^{-\Lambda' N_\Delta}}. \tag{39}$$

Approximate the exponentials as step functions to find

$$\langle \mathcal{O} \rangle \approx \frac{\mathcal{O}_1 + \mathcal{O}_2 + \cdots + 0 + 0}{1 + 1 + \cdots + 0 + 0} = \frac{1}{\mathcal{N}} \sum\nolimits_{n=1}^{\mathcal{N}} \mathcal{O}_n, \tag{40}$$

where $\mathcal{N}$ is the number of samples.

4.2. Phase transition

The Eq. (32) partition function Z_R describes a system that undergoes a phase transition. The partition function is roughly the number of accessible states at a given temperature. Here, the "temperature" is the inverse of the rescaled cosmological constant Λ'. The "entropy" or number of triangulations increases the partition function, while the "energy" or number of triangles per triangulation decreases the partition function. In fact, for high "temperatures" $\Lambda' < \Lambda'_c$, the partition function Z_R diverges to infinity, and for low "temperatures" $\Lambda' > \Lambda'_c$, the partition function Z_R converges to zero.

A toy model can reproduce some of the key results of the rigorous theory [22]. Focus on triangulations with distinct number of triangles, so that the simplified partition function

$$Z_s[\Lambda'] = \sum\nolimits_{N=1}^{\infty} e^{-\Lambda' N} = \frac{1}{e^{\Lambda'} - 1}, \tag{41}$$

which grows for small "hot" Λ', shrinks for large "cold" Λ', and for which $Z_s[\Lambda'_c] = 1$ implies the critical rescaled cosmological constant

$$\Lambda'_c = \ln 2 \approx 0.693. \tag{42}$$

In addition, if the averages

$$\langle N^k \rangle = \frac{1}{Z_s} \sum\nolimits_{N=1}^{\infty} N^k e^{-\Lambda' N}, \tag{43}$$

then the fractional fluctuation in universe size at Λ'_c is

$$\frac{\sqrt{\langle N^2 \rangle - \langle N \rangle^2}}{\langle N \rangle} = \left\langle \frac{\Delta N}{N} \right\rangle = \frac{1}{\sqrt{2}} \approx 0.707. \tag{44}$$

If the temporal size of the universe is fixed, this is also the fractional fluctuation of the spatial size or circumference of the universe.

4.3. Results

We implement a Monte Carlo simulation to study CDT in 1 + 1 dimensions. The simulation is coded in Objective-C using Xcode. A hash table records the neighboring triangles of each triangle. A regular array of triangles initializes the universe, which is rendered as a cylinder embedded in three dimensions with identified ends, as on the left of Fig. 7. Pseudo-random rearrangements of moves and inverse moves evolve the universe toward the Eq. (33) detailed balance, as on the right of Fig. 7. The two kinds of triangles (pointing toward the future or the past) should occur equally often and are coloured differently as a check.

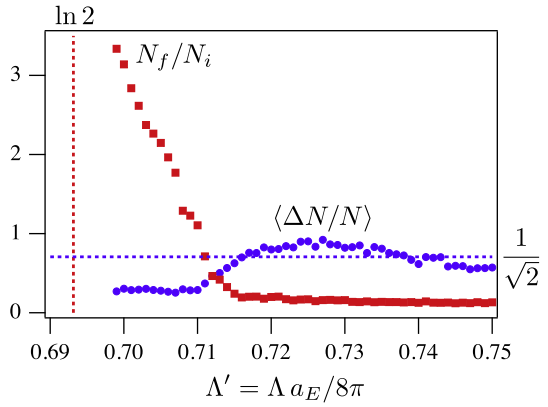

Fig. 8. Ratio of final to initial universe size (squares) and fractional fluctuations in circumference (disks) as a function of the rescaled cosmological constant just above the critical phase transition.

The simulation runs under Mac OS X on a single processor with 4 GB of RAM. A typical universe size has 32 time slices and 64 space steps for $32 \times 64 \times 2 = 4096$ total triangles. The simulation executes a transient of 10^5 rearrangements and then records 10^6 samples of the universe size each separated by 10^3 attempted rearrangements. By systematically varying the rescaled cosmological constant Λ', as summarised in Fig. 8, we confirm a phase transition near the Eq. (42) theory, where the universe size (in number of triangles) diverges. Our Metropolis algorithm success rate is about 30%, as about 70% of our proposed rearrangements are rejected. Nevertheless, we use the Eq. (40) averager to estimate the fractional fluctuation in universe circumference, which is in good agreement with the Eq. (44) theory for cosmological constants just above (and a little "colder" than) the critical value where the universe size is stable. Diverging (or converging) universes dampen the fluctuations.

5. Conclusion

A laptop computer can readily simulate a CDT quantum gravity model and test theoretical predictions. Although an empty 1 + 1 dimensional universe is trivial in some ways and has no classical limit, it does exhibit vacuum fluctuations in size, and from those vacuum fluctuations in 3 + 1 dimensions emerges classical spacetime. Adjusting the cosmological constant Λ to fix the size of our model universe recalls Einstein's original motivation for introducing it. Furthermore, constructing a quantum gravity model of such a toy universe introduces important ideas and techniques that are applicable to other approaches to quantum gravity and can be generalised to higher and more physically interesting dimensions.

Future improvements to the current simulation include optimising the Eq. (37) move probability to increase our Metropolis success rate, implementing free temporal boundary conditions for a cylindrical topology, and increasing the number of triangulations to better approach the thermodynamic limit. Extensions to higher dimensions involve increasing the number of basic building blocks and Monte Carlo rearrangements. For example, in 2 + 1 dimensions, 3 tetrahedrons can be rearranged in 5 different ways. In the absence of the Gauss–Bonnet theorem, higher dimensional curvature can be expressed as a sum of deficit angles in the Regge calculus. Future challenges to CDT include incorporating matter, black holes, and Big Bang cosmology.

Acknowledgment

We thank John Ramsay and Wooster's Copeland Fund for Independent Study.

References

[1] Ambjørn J, Jurkiewicz J, Loll R. Sci Am 2008;299(1):43–9.
[2] Loll R. Classical Quant Grav 2008;25(11):114006.
[3] Rovelli C. Quantum gravity. Cambridge University Press; 2004.
[4] Ambjørn J, Jurkiewicz J, Loll R. In: Murugan J, Weltman A, Ellis GFR, editors. Foundations of space and time: reflections on quantum gravity. Cambridge University Press; 2012. p. 321–37.
[5] Ambjørn J, Jurkiewicz J, Loll R. Phys Rev Lett 2004;93:131301.
[6] Ambjørn J, Jurkiewicz J, Loll R. Phys Rev D 2005;72:064014.
[7] Hořava P. Phys Rev Lett 2009;102:161301.
[8] Carlip S. In: Kowalski-Glikman J, Durka R, Szczachor M, editors. AIP conference proceedings. American Institute of Physics; 2009. p. 36–43.
[9] Ambjørn J, Jurkiewicz J, Loll R. Phys Rev Lett 2000;85:924–7.
[10] Benedetti D, Henson J. Phys Rev D 2009;80:124036.
[11] Misner CW, Thorne KS, Wheeler JA. Gravitation. W.H. Freeman and Company; 1973.
[12] Feynman RP, Hibbs AR, Styer DF. Quantum mechanics and path integrals. Dover Publications; 2010.
[13] Beau M. Eur J Phys 2012;33:1023–39.
[14] DeWitt BS. Phys Rev 1967;160:1113–48.
[15] Gray A. Modern differential geometry of curves and surfaces with mathematica. 2nd ed. CRC Press; 1998.
[16] Wick GC. Phys Rev 1945;96:1124–34.
[17] Saff EB, Snider AD. Fundamentals of complex analysis with applications to engineering and science. 3rd ed. Prentice Hall; 2003.
[18] Regge T. Nuovo Cim 1961;19:558–71.
[19] Alexander JW. Ann Math. Second Series 1930;31:292–320.
[20] Ambjørn J, Durhuus B, Jonsson T. Quantum geometry: a statistical field theory approach. Cambridge University Press; 1997.
[21] Metropolis N, Rosenbluth AW, Rosenbluth MN, Teller AH, Teller E. J Chem Phys 1953;21:1087–92.
[22] Ambjørn J, Anagnostopoulous KN, Loll R. Phys Rev D 1999;60:104035.